Journal of Magnetism and Magnetic Materials 498 (2020) 166258

Contents lists available at ScienceDirect

Journal of Magnetism and Magnetic Materials

journal homepage: www.elsevier.com/locate/jmmm

Research articles

Spin-flop coupling induced large coercivity enhancement in Fe/FeRh/W (110) bilayers across ferromagnetic–antiferromagnetic phase transition of FeRh alloy

P. Dróżdż[a,*], M. Ślęzak[a], K. Matlak[a], A. Kozioł–Rachwał[a], J. Korecki[a,b], T. Ślęzak[a]

[a] AGH University of Science and Technology, Faculty of Physics and Applied Computer Science, Aleja Adama Mickiewicza 30, 30-059 Kraków, Poland
[b] Jerzy Haber Institute of Catalysis and Surface Chemistry, Polish Academy of Sciences, 30-239 Kraków, Poland

ARTICLE INFO

Keywords:
Magnetism
Phase transition
Magnetic anisotropy
FeRh alloy
Thin films
Epitaxy

ABSTRACT

We report on the large coercivity enhancement in epitaxial Fe/FeRh bilayer grown on W(110). It is shown that the coercive field increases by almost an order of magnitude when the FeRh alloy undergoes a phase transition from the ferromagnetic to antiferromagnetic state. Analysis of temperature spin structure evolution of the FeRh alloy across the magnetic transition reveals that the observed coercivity enhancement is caused by the interfacial spin-flop coupling between Fe and the antiferromagnetic FeRh layer.

1. Introduction

The FeRh alloy with equiatomic composition reveals a temperature induced first-order magnetic transition from antiferromagnetic (AFM) to ferromagnetic (FM) state at a transition temperature close to 350 K [1–3]. Recently, low dimensional FeRh films exhibiting AFM ↔ FM transition have attracted a lot of attention, as they are important materials for new storage media applications, such as heat assisted magnetic recording (HAMR) [4,5], AFM memory resistor [6] and magnetic refrigerators [7]. Promising results for the HAMR applications were reported for the FePt/FeRh bilayers, where a significant (95%) coercivity change has been observed along with the temperature driven transition from the ferromagnetic to the antiferromagnetic state of the FeRh system [8]. The mechanism responsible for the coercivity change in FePt/FeRh system was formation of the exchange spring system upon the transition to the FM state of the FeRh alloy [4]. In the case of Fe/FeRh ribbons, where the Fe coercive field at AFM state of FeRh was only 130 Oe, the variation of the coercive field originates from the interfacial spin-flop coupling [9]. Similar results showing coercivity change accompanied by a negligible exchange bias were reported for Fe/FeRh and CoFe/FeRh grown on MgO, Al_2O_3 and Ge substrates [10–12].

In this report we show that in contrast to all above mentioned experiments that concerned systems with relatively thick, bulk-like FeRh layers, the large enhancement of the coercive field can be obtained along with FM ↔ AFM transition for few nanometers thick FeRh films coupled to an ultrathin iron layer. In our Fe/FeRh/W(110) bilayers the coercive field H_C increases by almost an order of magnitude reaching a value close to 1000 Oe, when the FeRh system undergoes transition from the FM state to AFM phase. Moreover, a temperature window of the coercivity enhancement can be tuned by the FeRh film thickness. The temperature hysteresis of the H_C(T) dependence indicates that observed coercivity enhancement is driven by the AFM ↔ FM phase transition in nearby FeRh sublayers.

2. Experimental details and structural studies

The ^{56}Fe/^{57}FeRh bilayers were grown on a W(110) substrate and characterized in situ under ultra-high vacuum. Ultrathin ^{57}FeRh layers with thickness of 50 Å and 100 Å were grown by elemental co-deposition at room temperature. Iron isotopes were evaporated from resistively heated BeO crucibles, whereas the heating of the Rh source was realized by electron bombardment. The nominal Rh atomic concentration established by adjustment of Fe and Rh evaporation rates (both in a range of Å/min) was approximately 54%. The samples were post-annealed at 850 K for 30 min to promote the formation of the desired B2 structure [13]. The epitaxial character of the FeRh film was proven by high quality LEED patterns that are shown in Fig. 1b together with a LEED pattern corresponding to the W(110) substrate (Fig. 1a). The both 50 Å and 100 Å thick FeRh layers were covered by the epitaxial 10 Å ^{56}Fe ultrathin film and annealed at 450 K for 10 min,

* Corresponding author.
E-mail address: piotr.drozdz@fis.agh.edu.pl (P. Dróżdż).

https://doi.org/10.1016/j.jmmm.2019.166258
Received 14 August 2019; Received in revised form 22 November 2019; Accepted 30 November 2019
Available online 02 December 2019

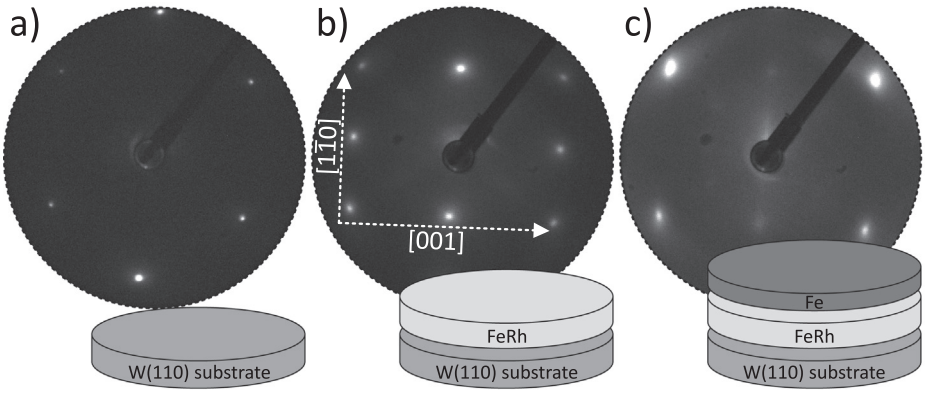

Fig.1. The LEED patterns collected with an electron beam energy of 65 eV for a) W(110) single crystal substrate, b) FeRh alloy film and c) Fe overlayer deposited on FeRh. White arrows indicate two orthogonally oriented in-plane directions, namely [001] and [1$\bar{1}$0].

leading to the formation of final structures denoted further as Fe/FeRh (50 Å) and Fe/FeRh (100 Å). The LEED pattern corresponding to the Fe surface exemplified in the Fig. 1c confirms an epitaxial growth of the Fe films on the FeRh layer.

3. Results and discussion

The magnetic properties were studied in-situ with longitudinal magneto-optical Kerr effect (LMOKE). We used a standard optical layout of LMOKE setup with s-polarized light (λ = 635 nm), photo-elastic modulation (f = 50 kHz) and lock-in detection. In such a case, the *2f* signal measured in the detector is proportional to the Kerr rotation [14]. To obtain a temperature dependence of magnetization, the LMOKE magnetic hysteresis loops were collected in a wide temperature range, and the Kerr rotation at saturation (denoted further as ROT_{SAT}) was taken as a measure of the magnetization in a similar way as in [15]. The exemplary magnetic hysteresis loops recorded during a heating process for the 100 Å thick FeRh single layer with an external magnetic field applied along the [001] in-plane direction, as well as the temperature profiles of AFM ↔ FM phase transitions are shown in Fig. 2a and 2b, respectively. All presented loops were normalized to the Kerr rotation at saturation derived from a loop measured at 350 K. It has to be noted that the LMOKE hysteresis curve measured with an external magnetic field applied along the [1$\bar{1}$0] in-plane direction (orthogonal to [001]) (see inset in Fig. 2a) is characterized by a lowered remanence value and a higher saturation field indicating a weak in-plane magnetic anisotropy of FeRh with the [001] easy magnetization axis. A similar weak in-plane anisotropy was observed for the single FeRh layer with a thickness of 50 Å.

The Fe growth was followed by the in-situ temperature dependent LMOKE measurements. The magnetic hysteresis loops collected with an external magnetic field applied along the [001] and [1$\bar{1}$0] directions are shown in Fig. 3a and b, respectively. Loops were collected at temperatures corresponding to the FM (350 K) and AFM (290 K) phases of the FeRh alloy (denoted further as $FeRh_{FM}$ and $FeRh_{AFM}$). At 350 K, the $Fe/FeRh_{FM}$ (100 Å) bilayer reveals uniaxial magnetic anisotropy with an easy axis along the [001] direction as it can be seen from the narrow rectangular hysteresis curve measured with external magnetic field applied parallel to the [001] direction and a typical hard axis loop acquired for the [1$\bar{1}$0] direction. At low temperature, corresponding to the AFM state, the uniaxial [001] magnetic anisotropy of the Fe overlayer persists as indicated by the rectangular hysteresis curve measured with an external magnetic field applied along [001] direction shown in blue in Fig. 3a. Simultaneously, the LMOKE loop measured with an external magnetic field applied along [1$\bar{1}$0] direction (not shown) was hard like, but even in a maximal available magnetic field the saturation state could not be reached. Similar magnetic anisotropy with [001] easy magnetization direction was observed for the Fe/FeRh (50 Å) bilayer.

The observed uniaxial magnetic anisotropy is typical for the Fe(110) films with a two-fold symmetry [16–19]. Which is more important, comparison of the loops measured for Fe/FeRh (100 Å) with external magnetic field applied along [001] at 290 K and 350 K clearly shows an increase of coercive field at low temperature. The systematic measurement of the LMOKE loops as a function of temperature were performed with an external magnetic field along the [001] direction. The temperature dependence of Kerr rotation at saturation, $ROT_{SAT}(T)$, as

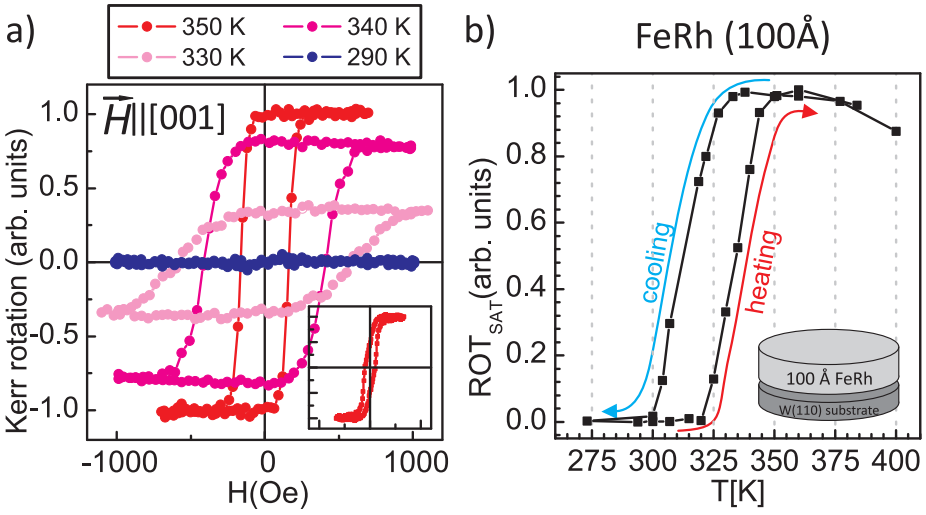

Fig. 2. a) Exemplary magnetic hysteresis loops collected for a 100 Å thick FeRh single layer during heating process. An external magnetic field was applied along the [001] in-plane direction. Inset shows a loop collected at 350 K for an external magnetic field along the [1$\bar{1}$0] direction. The scaling of the inset axes is the same range as in the main plot. b) Temperature dependences of Kerr rotation at saturation for a 100 Å thick FeRh single layer. Blue and red arrows indicate branches measured during cooling and heating process, respectively.

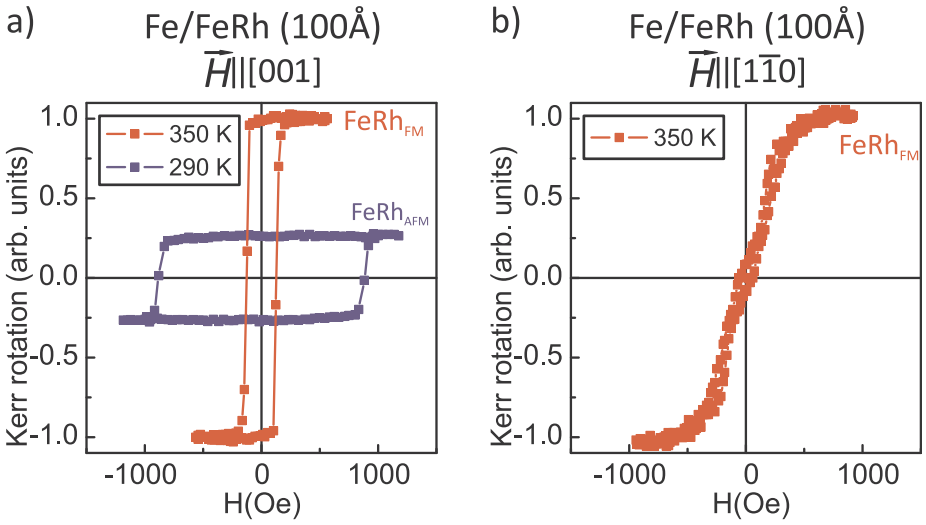

Fig. 3. Magnetic hysteresis loops collected for Fe/FeRh (100 Å) bilayer for external magnetic field applied along a) [001] and b) [1$\bar{1}$0] directions for temperatures corresponding to FM (350 K) and AFM (290 K) phase of the FeRh alloy.

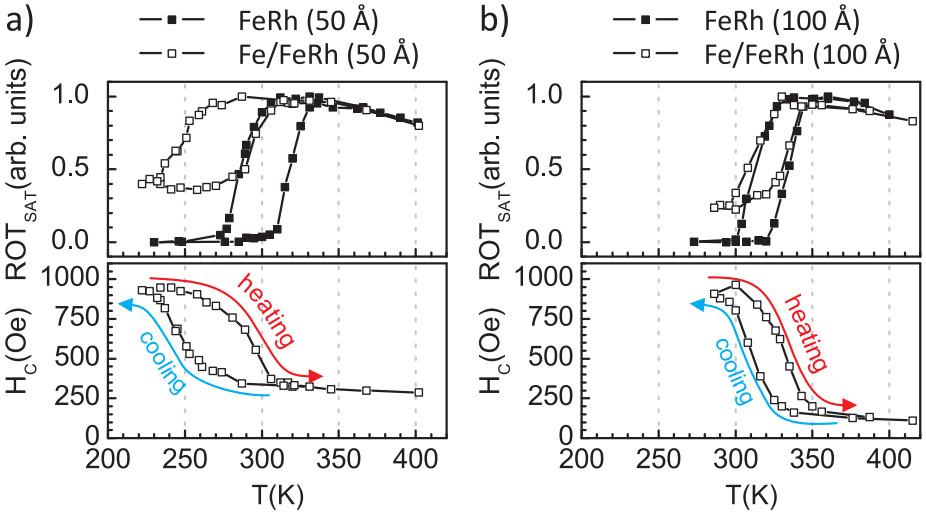

Fig. 4. Top panels of a) and b) show comparison of temperature profiles of AFM ↔ FM transitions between FeRh single layers (filled symbols) and Fe/FeRh bilayers (open symbols) for 50 Å and 100 Å thick FeRh alloy, respectively. Bottom panels show temperature dependences of the coercivity determined for the Fe/FeRh bilayers.

well as temperature dependence of coercivity, $H_C(T)$, derived from the loops measured for the Fe/FeRh (50 Å) and Fe/FeRh (100 Å) bilayers are shown in the Fig. 4a and 4b, respectively. The curves corresponding to the Fe/FeRh bilayers and FeRh single layers are marked by open and filled symbols, respectively. The presented $ROT_{SAT}(T)$ curves are normalized to its maximum value of ROT_{SAT}. In both cases, the temperature profile of the AFM ↔ FM transition is shifted to the lower values for the Fe/FeRh bilayers in comparison with the FeRh single layer, although this effect is more pronounced for the Fe/FeRh (50 Å) sample. Similar effect was previously observed for the Co/FeRh [20] system and interpreted as the influence of magnetic proximity of the FM (Co) film on the AFM ↔ FM transition in FeRh. Non-zero values of ROT_{SAT} at low temperatures for the Fe/$FeRh_{AFM}$ systems are associated with Kerr rotation corresponding to the top Fe layer.

The temperature dependence of coercivity for bilayers shown in the bottom panel of Fig. 4 reveals a systematic decrease and increase of H_C of Fe/FeRh bilayers during the heating and cooling process, respectively. The comparison of the $ROT_{SAT}(T)$ and $H_C(T)$ plots for the Fe/FeRh bilayers indicates that the observed changes of the coercive field are fully correlated with the magnetic AFM ↔ FM transitions in the FeRh alloy. The corresponding changes in the Kerr rotation and H_C occur at identical temperatures and are characterized by similar thermal hysteresis. In the case of Fe/FeRh (100 Å) bilayer the coercivity changes from about 100 Oe at the FM state of FeRh to nearly 1000 Oe for the AFM state of the FeRh alloy. For the Fe/FeRh/(50 Å) sample the maximal value of the coercive field also reaches 1000 Oe although the relative coercivity change is smaller. This can be explained by the influence of epitaxial strain on magnetization reversal of 50 Å FeRh at the FM state resulting in a higher coercivity of the Fe/FeRh (50 Å) bilayer. In addition, it is clear from our data that the temperature dependence of the coercivity can be controlled by the FeRh layer thickness as for the thinner FeRh layer the AFM ↔ FM transition is broader and shifted towards lower temperatures.

As the mechanism of the observed coercivity enhancement of Fe/FeRh at the AFM state we propose the interfacial spin-flop coupling [21]. Since our MOKE data clearly show that Fe magnetization does not switch upon cooling preserving its easy magnetization direction along [001] direction a spin flop phenomenon must consist in the switching of FeRh spins from [001] to the [1$\bar{1}$0] direction when FeRh passes from the FM to AFM state. The comparison of the spin structure of Fe/FeRh system at FM and AFM state of FeRh is schematically shown in the Fig. 5c. Such an effect was previously observed in FM/AFM interfaces with a two-fold symmetry such as for example Fe(110)/Fe_2F [22] and it was correlated with negligible or zero exchange bias effect. Similarly, in our Fe/FeRh systems, at all temperatures the hysteresis curves were perfectly symmetric indicating the absence of the exchange bias effect.

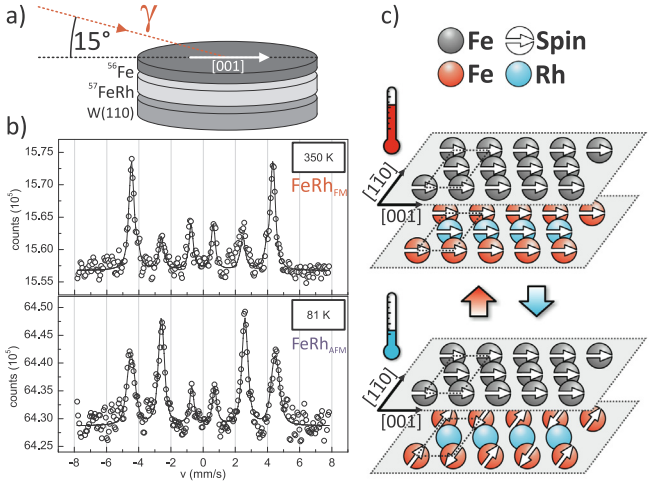

Fig. 5. a) Geometry of the grazing CEMS setup. The [001] in-plane direction is marked by white arrow. b) CEMS spectra collected for the $^{56}Fe/^{57}FeRh$ (100 Å) bilayer at temperatures corresponding to the FM (350 K) and AFM (81 K) state in top and bottom panel, respectivly. c) The comparison of the spin structure of Fe/FeRh system at FM and AFM state of FeRh.

According to the theoretical calculations of Schutles et al. [21] for perfectly compensated AFM/FM interface orthogonal exchange coupling does not lead to exchange bias but instead is responsible for enhancement of the coercivity. In phenomenological description of the interface exchange interaction between AFM and FM the bilinear and biquadratic (spin-flop) exchange coupling contributions (J_1 and J_2, respectively) can be assumed as proposed by Xu et al. [23]. In our case the absence of exchange bias at AFM state of the FeRh means $J_1 = 0$ and J_2 spin-flop coupling favours perpendicular alignment between AFM and FM spins giving a rise to the uniaxial magnetic anisotropy responsible for the enhancement of the coercivity. Similarly, convincing evidences about the key role of spin-flop coupling as a direct source of induced uniaxial magnetic anisotropy in AFM/FM systems can be also found in [21,24]. At the FM state of the FeRh the J_2 is zero as the frustration of the exchange interaction vanishes and J_1 favours FM coupling between Fe and FeRh sublayers.

Direct confirmation of the spin flop coupling effect is provided by temperature dependent in-situ conversion electron Mössbauer spectroscopy (CEMS). CEMS method allows to get insight into the spin structure evolution of the FeRh alloy for both AFM and FM phases as reported in [25–28]. CEMS spectra were collected for $^{56}Fe/^{57}FeRh/$ (100 Å) in grazing incidence geometry, where the angle between the direction of incoming γ-rays and sample surface was 15°, and with the [001] in-plane direction of Fe/FeRh aligned in the plane of incidence (see Fig. 5a). Owing to the isotopic sensitivity of CEMS the thermal evolution FeRh spin orientation in the Fe/FeRh bilayer could be selectively followed. Collected spectra were analysed using commercial software and the fitting procedure was based on the hyperfine magnetic field distribution represented by a sum of Gaussian components [29]. The orientation of the magnetic hyperfine field that is antiparallel to the local spin direction was determined by the intensity ratio $R_{2/3}$ of the second and third line in the Mössbauer six-line spectrum using a simple formula:

$$R_{2/3} = 4sin^2\,\theta/(1 + cos^2\,\theta),$$

where θ is the angle between magnetization and direction of incoming γ-rays.

The CEMS spectra were collected for Fe/FeRh (100 Å) bilayer at temperatures corresponding to the FM (350 K) and AFM (81 K) state of the FeRh alloy. Spectrum collected for the FM phase of FeRh (top panel on Fig. 5b) can be fitted with a single magnetic sextet, reflecting a high degree of magnetic and structural homogeneity of the FeRh system. The hyperfine field value derived from the fit is equal to 27.3 T and the intensity ratio $R_{2/3}$ is approximately 0.7. Considering the measurement geometry, this $R_{2/3}$ value indicates a uniaxial magnetic anisotropy of $FeRh_{FM}$ with an easy axis along the [001] in-plane direction, in agreement with the MOKE results. The CEMS spectrum collected for the $Fe/FeRh_{AFM}$ state is shown in the bottom panel of Fig. 5b. The most pronunced change between the CEMS spectra collected for the FM and AFM state of the alloy consists in the increase of R_{23} ratio to 3.6 value indicating the reorientation of the FeRh spins from [001] direction at FM state to [1$\bar{1}$0] for AFM phase. This observation, in combination with the MOKE data indicating the [001] easy magnetization direction of the Fe overlayer at both FM and AFM states of FeRh (see rectangular loops in Fig. 3a) directly proves a spin flop coupling occurring along with the transition of FeRh to the AFM state.

4. Conclusion

In conclusion, we showed a large temperature induced coercivity changes in epitaxial Fe/FeRh bilayers grown on W(110) substrate. The temperature hysteresis of the $H_C(T)$ dependence indicates that the observed coercivity enhancement is driven by the AFM ↔ FM phase transitions in the nearby FeRh sublayers. Direct analysis of temperature evolution of the spin structure in the FeRh reveals that the observed coercivity enhancement is caused by a spin-flop coupling at the $Fe/FeRh_{AFM}$ interface.

CRediT authorship contribution statement

P. Dróżdż: Investigation, Formal analysis, Writing - original draft, Visualization. **M. Ślęzak:** Investigation, Validation. **K. Matlak:** Software, Data curation. **A. Kozioł–Rachwał:** Investigation, Validation. **J. Korecki:** Writing - review & editing, Supervision. **T. Ślęzak:** Conceptualization, Writing - review & editing, Supervision, Funding acquisition.

Declaration of Competing Interest

The authors declare that they have no known competing financial interests or personal relationships that could have appeared to influence the work reported in this paper.

Acknowledgments

This work is supported by the National Science Center Poland under Project No. 2015/19/B/ST3/00543 and partially by the AGH University of Science and Technology statutory task No. 11.11.220.01/6 within subsidy of the Ministry of Science and Higher Education. J. Korecki thanks for support from statutory research funds of ICSC PAS.

References

[1] J.S. Kouvel, C.C. Hartelius, Anomalous magnetic moments and transformations in the ordered alloy FeRh, J. Appl. Phys. 33 (1962) 1343.
[2] M. Fallot, Les Alliages Du Fer Avec Les Métaux de La Famille Du Platine, Ann. Phys. 10 (1938) 291.
[3] M. Fallot, R. Hocart, Sur L'apparition Du Ferromagnétisme Par Élévation de Température Dans Des Alliages de Fer et de Rhodium, Rev. Sci. 77 (1939) 498.
[4] J. Thiele, S. Maat, E.E. Fullerton, FeRh/FePt exchange spring films for thermally assisted magnetic recording media, Appl. Phys. Lett. 82 (2003) 2859.
[5] M.H. Kryder, E.C. Gage, T.W. Mcdaniel, W.A. Challener, R.E. Rottmayer, G. Ju, Y.T. Hsia, M.F. Erden, Heat assisted magnetic recording, Proc. IEEE 96 (2008) 1810.
[6] X. Marti, I. Fina, C. Frontera, J. Liu, P. Wadley, Q. He, R.J. Paull, J.D. Clarkson, J. Kudrnovský, I. Turek, J. Kuneš, D. Yi, J. Chu, C.T. Nelson, L. You, E. Arenholz, S. Salahuddin, J. Fontcuberta, T. Jungwirth, R. Ramesh, Room-temperature antiferromagnetic memory resistor, Nat. Mater. 13 (2014) 367.
[7] E. Stern-Taulats, A. Planes, P. Lloveras, M. Barrio, J.L. Tamarit, S. Pramanick, S. Majumdar, C. Frontera, L. Mañosa, Barocaloric and magnetocaloric effects in $Fe_{49}Rh_{51}$, Phys. Rev. B 89 (2014) 214105.
[8] N.T. Nam, W. Lu, T. Suzuki, Exchange Bias of Ferromagnetic/antiferromagnetic in FePt/FeRh Bilayers, J. Appl. Phys. 105 (2009) 07D708.

[9] V. Kuncser, W. Keune, B. Sahoo, E. Duman, M. Acet, F. Radu, M. Valeanu, O. Crisan, G. Filoti, Magnetic interactions and spin configuration in FeRh and Fe/FeRh systems, J. Magn. Magn. Mater. 272–276 (2004) 348.
[10] I. Suzuki, Y. Hamasaki, M. Itoh, T. Taniyama, Controllable exchange bias in Fe/metamagnetic FeRh bilayers, Appl. Phys. Lett. 105 (2014) 172401.
[11] S. Yamada, K. Tanikawa, J. Hirayama, T. Kanashima, T. Taniyama, K. Hamaya, Low-temperature B2 ordering and magnetic properties of $Fe_{100-x}Rh_x$ films on Bcc alloys, Phys. Rev. B 92 (2015) 094416.
[12] S. Yamada, K. Tanikawa, J. Hirayama, T. Kanashima, T. Taniyama, K. Hamaya, Exchange coupling in metallic multilayers with a Top FeRh layer, AIP Adv. 6 (2016) 056115.
[13] S.K. Kim, Y. Tian, F. Jona, P.M. Marcus, Atomic structure of a 110 surface of the FeRh alloy, Phys. Rev. B 56 (1997) 9858.
[14] P. Vavassori, Polarization modulation technique for magneto-optical quantitative vector magnetometry, Appl. Phys. Lett. 77 (2000) 1605.
[15] P. Dróżdż, M. Ślęzak, K. Matlak, D. Wilgocka-Ślęzak, J. Korecki, T. Ślęzak, K. Matlak, Temperature controlled Fe/Au/FeRh spin valves, AIP Adv. 8 (2018) 101434.
[16] U. Gradmann, J. Korecki, G. Waller, In-plane magnetic surface anisotropies in Fe (110), Appl. Phys. A 39 (1986) 101.
[17] T. Ślezak, M. Zajac, M. Ślezak, K. Matlak, A. Kozioł-Rachwał, D. Wilgocka-Ślezak, A.I. Chumakov, R. Rüffer, J. Korecki, Different scenarios for the in-plane spin reorientation transition in Fe(110) films on W(110), Phys. Rev. B 87 (2013) 094423.
[18] T. Ślęzak, M. Ślęzak, M. Zając, K. Freindl, A. Kozioł-Rachwał, K. Matlak, N. Spiridis, D. Wilgocka-Ślęzak, E. Partyka-Jankowska, M. Rennhofer, A.I. Chumakov, S. Stankov, R. Rüffer, J. Korecki, Noncollinear magnetization structure at the thickness-driven spin-reorientation transition in epitaxial Fe films on W(110), Phys. Rev. Lett. 105 (2010) 027206.
[19] M. Slęzak, T. Ślęzak, K. Matlak, B. Matlak, P. Dróżdż, T. Giela, D. Wilgocka-Ślęzak, N. Pilet, J. Raabe, A. Kozioł-Rachwał, J. Korecki, Giant in-plane magnetic anisotropy in epitaxial Bcc Co/Fe (110) bilayers, Phys. Rev. B 94 (2016) 014402.
[20] P. Dróżdż, M. Ślęzak, K. Matlak, B. Matlak, K. Freindl, D. Wilgocka-Ślęzak, N. Spiridis, J. Korecki, T. Ślęzak, Switching of Co magnetization driven by antiferromagnetic-ferromagnetic phase transition of FeRh alloy in Co/FeRh bilayers, Phys. Rev. Appl. 9 (2018) 034030.
[21] T. Schulthess, W. Butler, Consequences of spin-flop coupling in exchange biased films, Phys. Rev. Lett. 81 (1998) 4516.
[22] T.J. Moran, J. Nogués, D. Lederman, I.K. Schuller, D. Lederman, I.K. Schuller, Perpendicular coupling at Fe – FeF_2 interfaces, Appl. Phys. Lett. 72 (1998) 617.
[23] X. Xu, J. Hu, Surface science spin-flop coupling and exchange anisotropy in ferromagnetic/antiferromagnetic bilayers, Surf. Sci. 603 (2009) 814.
[24] W. Zhang, M. Krishnan, Field and temperature-driven magnetic reversal of spin-flop coupled epitaxial Fe/Mn Pd bilayers, 88, 024428 (2013).
[25] C. Bordel, J. Juraszek, D.W. Cooke, C. Baldasseroni, S. Mankovsky, J. Minar, Fe Spin reorientation across the metamagnetic transition in strained FeRh thin films, Phys. Rev. Lett. 109 (2012) 117201.
[26] G. Shirane, C.W. Chen, P.A. Flinn, R. Nathans, Hyperfine fields and magnetic moments in the Fe-Rh system, J. Appl. Phys. 34 (1963) 1044.
[27] J. van Driel, R. Coehoorn, G.J. Strijkers, E. Bruck, F.R. Boer, Compositional dependence of the giant magnetoresistance in thin films FeRh, J. Appl. Phys. 85 (1999) 1026.
[28] G. Shirane, C.W. Chen, P.A. Flinn, R. Nathans, Mossbauer Study of Hyperfine Fields and Isomer Shifts in the Fe-Rh Alloys, Phys. Rev. 131 (1963) 183.
[29] K. Lagarec, Recoil 1.05 Mössbauer Analysis Software for Windows, © 1998, (2002).